American Mineralogist, Volume 81, pages 1501–1506, 1996

Crystal structures of the {011}, {610}, and {010} growth sectors in brewsterite

MIZUHIKO AKIZUKI, YASUHIRO KUDOH, AND TAKAHIRO KURIBAYASHI

Institute of Mineralogy, Petrology, and Economic Geology, Faculty of Science, Tohoku University, Sendai 980, Japan

ABSTRACT

Crystal structures were determined by single-crystal X-ray methods for the {011}, {610}, and {010} growth sectors of brewsterite from Strontian, Scotland. Refinements (R_w = 4.3–6.6%) showed that all three growth sectors are triclinic and that their structures differ slightly.

INTRODUCTION

Brewsterite, a rare strontium zeolite [$(Sr,Ba)_2Al_2Si_{12}O_{32}\cdot 10H_2O$] was first found in Strontian, Scotland, by Brooke (1822). Des Cloizeaux (1874) performed optical studies of brewsterite from Strontian and under crossed polars found that the (010) section was divided into three sectors. The crystal structure of brewsterite from Strontian was determined in monoclinic space group $P2_1/m$ by Perrotta and Smith (1964) and later refined in the same space group by Schlenker et al. (1977). Recently, Ba-dominant brewsterite, space group $P2_1/m$ or $P2_1$, was found in two localities (Robinson and Grice 1993; Cabella et al. 1993).

Akizuki (1987a) studied the relationship between optical properties and the {610}, {011}, and {010} growth sectors of brewsterite from Strontian, Scotland. The (610) face consisted of striations parallel to the c axis. In a (001) thin section, the {610} sector showed extinction inclined about 2–3° from the b axis, which suggests that the {610} sector is triclinic. The (011) face showed fine striations parallel to the a axis. Optical extinctions of the four {011} sectors in the (100) thin section are also inclined relative to the b axis, which shows that the four {011} sectors are also triclinic and comprise a fourling sectoral twin about the a axis. The (010) face was found to consist of (0kl) and (0k$\bar{l}$) vicinal faces with fine steps parallel to the a axis but without a growth center. In addition, the {0kl} and {0$k\bar{l}$} sectors corresponding to the vicinal faces are related by a triclinic twin. These optical observations suggest that the brewsterite sample from Strontian is triclinic in the {610}, {011}, and {010} sectors, although optical orientations and $2V$ values differ among the sectors.

Akizuki (1987a) explained the origin of the triclinic sectors in brewsterite by a local charge balance on the growth steps on the crystal faces. Akizuki (1987b) suggested a general mechanism for the formation of structurally distinct sectors in zeolites and other minerals.

The purpose of the present study is to confirm the crystal structures of the optically triclinic {610}, {011}, and {010} growth sectors from the brewsterite crystal from Strontian, Scotland. In addition, we describe the structural differences between the sectors.

SAMPLE

The form of the brewsterite crystal from Strontian is shown in Figure 1. Thin sections parallel to the (010) and (100) faces show the {610}, {011}, and {010} structural sectors (cf. Akizuki 1987a). Backscattered electron imaging shows compositional growth zoning with respect to the Ba/Sr ratio (Fig. 2), suggesting that the chemical composition varied during growth. The chemical compositions of the three sectors were determined by electron-probe microanalysis. The atomic ratio Ba/(Ba + Sr) varies from 0.62 to about 0.5 at the rim, although the ratio is as low as 0.33 in some growth bands, and from about 0.5 to 0.23 at the core. Compositions of the three sectors, including maximum and minimum values of the atomic ratio Ba/(Ba + Sr), are given in Table 1. The atomic abundances of Ca, Na, and K are <1%.

EXPERIMENTAL METHODS

For structure analyses, single crystals were hand-picked from the {610}, {011}, and {010} sectors in a section parallel to the (010) face. Unit-cell parameters were obtained by least-squares fitting of the positions of centered reflections (25 reflections ranging from 40.9 to 52.6° 2θ for the {011} sector, 25 reflections ranging from 21.6 to 28.5° for the {610} sector, and 24 reflections ranging from 40.8 to 54.6° for the {010} sector); refined values are given in Table 2.

Intensity data were measured at room temperature using the ω-2θ scan method, with a maximum 2θ value of 55.0°, on an automated four-circle single-crystal X-ray diffractometer (Rigaku AFC-7S) with graphite-monochromatized Mo$K\alpha$ radiation (λ = 0.71069 Å). Lorentz and polarization corrections were applied, but no absorption corrections were made because of the small sizes of the crystals (0.18 × 0.18 × 0.12 mm for the {011} and {010} sectors, 0.13 × 0.12 × 0.09 mm for the {610} sector) and the moderate absorption coefficients (30.4, 29.6, and 30.8 cm^{-1} for the {011}, {610}, and {010} sectors, respectively). Starting atomic coordinates for the triclinic refinements were derived from the monoclinic structure refinement of Schlenker et al. (1977). Individual reflections were assigned weights $w = 1/\sigma^2$. All calcula-

0003–004X/96/1112–1501$05.00

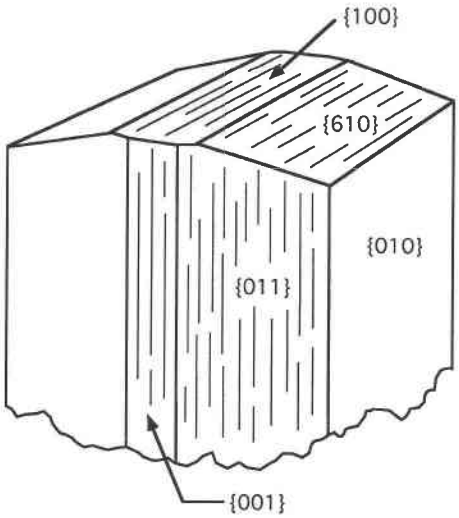

FIGURE 1. Crystal form of brewsterite from Strontian, Scotland.

tions were performed using the teXsan crystallographic software package of Molecular Structure Corporation (1985, 1992). Structure refinement information is given in Table 3.

The atomic coordinates and anisotropic displacement parameters are listed in Tables 4 and 5.[1] Selected interatomic distances and angles are summarized in Table 6. Al contents in the tetrahedral sites were estimated by two methods. The method of Smith (1974) estimates the Al occupancy of the T sites on the basis of the T-O distances. The method of Artioli et al. (1985) uses both the T-O distance and the T-O-T angle to estimate the Al occupancy. The Al occupancies estimated by both methods are given in Table 7. Occupancies of Al in tetrahedral sites were not refined. Si (neutral scattering factors) was assigned to T sites. Observed and calculated structure factors for the {011}, {610}, and {010} sectors are available from the authors upon request.

[1] A copy of Table 5 may be ordered as Document AM-96-629 from the Business Office, Mineralogical Society of America, 1015 Eighteenth Street NW, Suite 601, Washington, DC 20036, U.S.A. Please remit $5.00 in advance for the microfiche.

TABLE 1. Chemical formulas determined by EPMA

	Si/Al	Chemical formula
{011} sector	3.09	$(Sr_{0.50}Ba_{0.45}K_{0.01})Al_{1.96}Si_{6.06}O_{16}\cdot nH_2O$
{610} sector	2.88	$(Sr_{0.40}Ba_{0.55}K_{0.01})Al_{2.07}Si_{5.97}O_{16}\cdot nH_2O$
{010} sector	3.09	$(Sr_{0.67}Ba_{0.24}K_{0.01})Al_{1.96}Si_{6.06}O_{16}\cdot nH_2O$
Schlenker et al. (1977)	2.90	$(Sr_{1.42}Ba_{0.48}K_{0.02})Al_{4.12}Si_{11.95}O_{32}\cdot nH_2O$

Note: Bulk-chemical formula range is from $(Sr_{0.33}Ba_{0.62}K_{0.01}Ca_{0.01}Na_{0.01})Al_{2.10}Si_{5.95}O_{16}\cdot nH_2O$ (maximum Ba content) to $(Sr_{0.77}Ba_{0.23}K_{0.01}Ca_{0.01}Na_{0.01})Al_{2.03}Si_{5.98}O_{16}\cdot nH_2O$ (minimum Ba content). Chemical formulas of the {011}, {610}, and {010} sectors are based on 2, 3, and 2 points average, respectively, and estimated deviations of Sr, Ba, and K are 0.02, 0.02, 0.01, respectively.

The structures of the three sectors were refined in both triclinic and monoclinic symmetries. The *R* factors were smaller by about 2% in the triclinic refinements than in the monoclinic ones. The calculated Al occupancies are clearly different in some T sites, especially in the TD and TD′ sites of the {001} sector and in the TC and TC′ sites of the {610} sector.

RESULTS AND DISCUSSION

The present study confirms that the structures of the {011}, {610}, and {010} sectors of brewsterite from Strontian are triclinic. Al occupancies, which are schematically shown in Figure 3, are not symmetrical with respect to the morphological mirror plane in the {011}, {610}, and {010} sectors. The TD tetrahedron, which is not directly coordinated with the large cation (Sr and Ba), may contain a small amount of Al in the {011} sectors. Also, in another specimen from the same locality, the Al

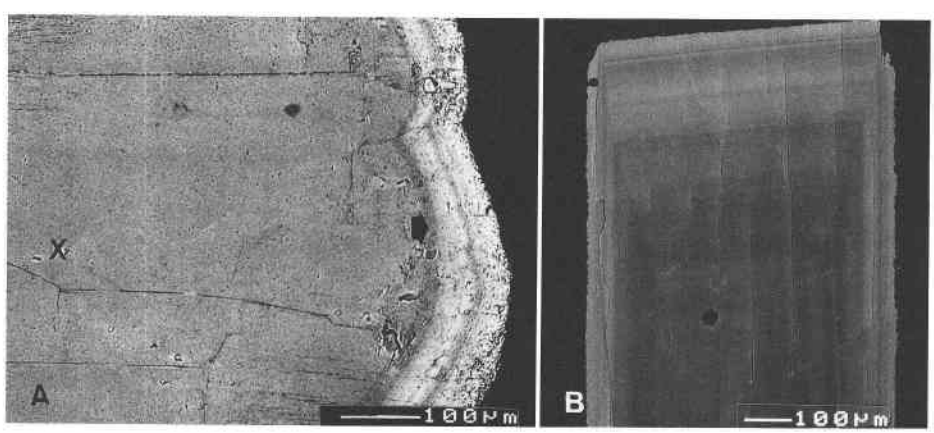

FIGURE 2. Backscattered electron images of brewsterite. (**A**) The *a* axis is normal to the photograph, and the *b* axis is horizontal. The X shows the center of the crystal in the section. The lighter rim is richer in Ba than the darker core; the rim consists of four layers. The narrow dark layer indicated by the arrow is the richest in Sr. (**B**) The *b* axis is normal, and the *a* axis is vertical. The section in **B** corresponds to the rim.

TABLE 2. Cell parameters

	a (Å)	*b* (Å)	*c* (Å)	α (°)	β (°)	γ (°)
{011} sector*	6.782(1)	17.510(3)	7.740(1)	89.90(1)	94.09(1)	90.10(1)
{610} sector**	6.779(1)	17.530(2)	7.750(2)	89.98(1)	94.49(2)	90.13(2)
{010} sector†	6.785(1)	17.546(2)	7.740(1)	89.98(1)	94.25(1)	90.06(1)
Schlenker et al. (1977)	6.793(2)	17.573(6)	7.759(2)		94.54(3)	
JCPDS	6.779(2)	17.520(3)	7.749(2)		94.47(1)	

* Using 25 reflections in the range $40.9° < 2\theta < 52.6°$.
** Using 25 reflections in the range $21.6° < 2\theta < 28.5°$.
† Using 24 reflections in the range $40.8° < 2\theta < 54.6°$.

occupancies of the TD and TD′ sites are 10 and 0% in the {011} sector, respectively.

Perrotta and Smith (1964) and Schlenker et al. (1977) showed that the Sr cation and three H_2O molecules are situated on the mirror plane in space group $P2_1/m$. However, they did not take the different sectors into consideration. Sr is directly coordinated by four framework O atoms and five H_2O molecules in the {011}, {610}, and {010} sectors of the present specimen. The coordination is the same in both the triclinic and monoclinic models. The Sr position is shifted in the triclinic refinement with respect to its ideal position in monoclinic symmetry with $\Delta x = -0.0015$, $\Delta y = 0.0001$, and $\Delta z = -0.0030$. The distances Sr-O2 = 2.815(5) and Sr-O′2 = 2.809(5) Å in the {011} sector are slightly shorter than the Sr-O2 = 2.831(4) Å value (Schlenker et al., 1977) of the monoclinic model. There were no significant differences between Sr-O distances in the triclinic and monoclinic models in the {610} and {010} sectors.

On the basis of studies of the relationships between the surface features and internal textures of many minerals such as zeolites and adularia, Akizuki (1981a, 1981b) and Akizuki and Konno (1985) explained the origin of anomalous optical properties, internal textures, and reduced symmetry in sectors as a product of ordering on the side faces of growth steps. Akizuki (1987b) suggested the following general mechanism for the formation of growth sectors. Although a crystal consists of a three-dimensional structure, it is produced by superposition of a two-dimensional atomic arrangement. According to Pauling's second rule, the local charge balance must be maintained in a three-dimensional structure. Tetrahedra that are directly coordinated by alkali ions are preferentially occupied by Al in zeolites (e.g., Schlenker et al. 1977; Perrotta 1967). The electrostatic charge on the growth surface, however, is not balanced in the direction perpendicular to the surface, and therefore an ionic crystal can grow continuously.

The charge balance must be maintained along the two-dimensional structure exposed on the growth surface as well as within the crystal. The two-dimensional atomic arrangements exposed on the growth step of the surface of an aluminosilicate differ among nonequivalent surfaces, such as (011) and (610) of brewsterite. If the tetrahedral growth unit is added to a step after a large cation site is filled, Al^{3+} is predicted to occupy the tetrahedron preferentially, whereas if the tetrahedral unit is added prior to the cation, Si^{4+} should preferentially occupy the site. Thus, the degree of the Al-Si ordering may differ among sectors. If the growth-step orientation is normal to a mirror or glide plane, the two sites related by the symmetry plane are equivalent on the step surface, resulting in disordered Al-Si arrangements. Conversely, if the step edge is inclined to a symmetry plane, the two sites that are equivalent in the crystal are not equivalent on the step surface. Thus, ordering can occur and the symmetry of the crystal may be reduced. The morphological symmetry plane changes into a twin plane if the symmetry is reduced because of ordering.

The origin of the triclinic symmetry of the {011}, {610}, and {010} sectors of brewsterite may be explained by this mechanism. Because the (011) face is inclined toward the (010) mirror plane, the Al occupancies of the T and T′ sites, which are symmetrically related with respect to the mirror plane, are not equivalent in the {011} sector, resulting in triclinic symmetry (Akizuki 1987a). In addition, the TD and TD′ tetrahedra, which are not directly coordinated with Sr and Ba, are slightly occupied by Al. This suggests that the growth kinetics are complex on the rough surface during growth.

TABLE 3. Refinement information for {011}, {610}, and {010} sectors

Sector	{011}	{610}	{010}
Dimension of crystal (mm)	0.18 × 0.18 × 0.12	0.13 × 0.12 × 0.09	0.18 × 0.18 × 0.12
Refinement space group	$P\bar{1}$	$P\bar{1}$	$P\bar{1}$
Scan type	ω-2θ	ω-2θ	ω-2θ
Unique reflections	4202	4208	4211
Reflections used in the refinement ($I > 3\sigma_I$)	3357	3044	3613
R value (%)*	5.0	4.3	5.3
R_w value (%)**	4.7	4.3	6.6

* $R = \Sigma||F_o| - |F_c||/\Sigma|F_o|$.
** $R_w = [\Sigma_w(|F_o| - |F_c|)^2/\Sigma_w F_o^2]^{1/2}$.

TABLE 4. Atomic coordinates of {011}, {610}, and {010} sectors

Atom	x	y	z	B_{eq} (Å²)
		{011} sector		
TA	0.3166(3)	0.0791(1)	0.8224(2)	0.99(4)
TA′	0.3163(3)	0.4208(1)	0.8227(3)	1.05(4)
TB	0.4117(3)	0.0582(1)	0.2095(3)	1.01(4)
TB′	0.4102(3)	0.4417(1)	0.2109(3)	0.99(4)
TC	0.5547(3)	0.1582(1)	0.5325(2)	0.91(4)
TC′	0.5541(3)	0.3417(1)	0.5344(2)	0.91(4)
TD	0.9045(3)	0.0520(1)	0.6416(3)	0.99(4)
TD′	0.9043(3)	0.4480(1)	0.6412(3)	0.94(4)
O1	0.3542(7)	0.1052(3)	0.0279(6)	1.4(1)
O1′	0.3518(7)	0.3950(3)	0.0308(6)	1.4(1)
O2	0.4289(7)	0.1255(3)	0.3537(6)	2.0(1)
O2′	0.4259(7)	0.3745(3)	0.3550(6)	2.0(1)
O3	0.7811(7)	0.1219(3)	0.5454(6)	1.7(1)
O3′	0.7807(7)	0.3786(3)	0.5466(6)	1.5(1)
O4	0.4414(8)	0.1385(3)	0.7080(6)	1.9(1)
O4′	0.4419(8)	0.3609(3)	0.7092(6)	2.0(1)
O5	0.0774(7)	0.0898(3)	0.7711(7)	2.1(1)
O5′	0.0758(7)	0.4104(3)	0.7691(7)	2.0(1)
O6	0.2348(8)	0.9985(3)	0.2444(7)	2.6(1)
O6′	0.2346(8)	0.5014(3)	0.2485(7)	2.5(1)
O7	0.3807(7)	0.9888(3)	0.7987(6)	1.3(1)
O7′	0.3822(7)	0.5115(3)	0.7986(6)	1.4(1)
O8	0	0	½	2.9(2)
O8′	0	½	½	2.8(2)
O9	0.5688(9)	0.2501(3)	0.5044(7)	2.6(1)
M	0.24861(9)	0.25009(4)	0.17502(8)	1.74(1)
O10	0.0569(10)	0.2503(4)	0.4667(8)	3.7(2)
O11	0.9340(10)	0.1465(4)	0.1446(9)	4.8(2)
O11′	0.9302(10)	0.3535(4)	0.1458(10)	4.8(2)
O12	0.5996(9)	0.2504(4)	0.0289(9)	4.1(2)
O13	0.081(1)	0.2499(3)	0.8619(8)	4.0(2)
		{610} sector		
TA	0.3218(3)	0.0806(1)	0.8229(2)	0.95(4)
TA′	0.3205(3)	0.4185(1)	0.8223(2)	0.95(4)
TB	0.4060(3)	0.0568(1)	0.2115(2)	1.09(4)
TB′	0.4055(3)	0.4432(1)	0.2105(2)	1.09(4)
TC	0.5560(3)	0.1583(1)	0.5340(2)	1.01(4)
TC′	0.5542(3)	0.3421(1)	0.5333(2)	0.90(4)
TD	0.9085(3)	0.0528(1)	0.6407(2)	0.94(4)
TD′	0.9077(3)	0.4472(1)	0.6411(2)	0.90(4)
O1	0.3506(7)	0.1045(3)	0.0288(6)	1.5(1)
O1′	0.3494(7)	0.3936(3)	0.0285(6)	1.4(1)
O2	0.4234(7)	0.1243(3)	0.3592(6)	2.0(1)
O2′	0.4218(7)	0.3761(3)	0.3619(6)	1.9(1)
O3	0.7855(7)	0.1216(3)	0.5463(6)	1.8(1)
O3′	0.7806(7)	0.3797(3)	0.5449(6)	1.5(1)
O4	0.4497(7)	0.1406(3)	0.7160(6)	1.8(1)
O4′	0.4501(7)	0.3589(3)	0.7120(6)	1.8(1)
O5	0.0848(7)	0.0900(3)	0.7637(6)	2.0(1)
O5′	0.0834(7)	0.4076(3)	0.7606(6)	1.9(1)
O6	0.2250(8)	0.9967(3)	0.2412(7)	2.6(1)
O6′	0.2213(8)	0.5030(3)	0.2389(7)	2.5(1)
O7	0.3854(7)	0.9912(3)	0.7948(6)	1.6(1)
O7′	0.3847(7)	0.5081(3)	0.7961(6)	1.5(1)
O8	0	0	½	3.0(2)
O8′	0	½	½	2.8(2)
O9	0.5715(8)	0.2512(3)	0.4991(7)	2.4(1)
M	0.24969(8)	0.25010(3)	0.17711(7)	1.60(1)
O10	0.0580(9)	0.2507(3)	0.4700(7)	3.6(2)
O11	0.9285(9)	0.1461(4)	0.1506(9)	4.9(2)
O11′	0.9252(10)	0.3543(4)	0.1493(10)	5.2(2)
O12	0.6031(9)	0.2490(4)	0.0238(8)	4.1(2)
O13	0.0639(10)	0.2494(3)	0.8631(7)	3.8(2)
		{010} sector		
TA	0.3192(3)	0.0797(1)	0.8229(3)	1.38(5)
TA′	0.3187(3)	0.4201(1)	0.8230(3)	1.39(5)
TB	0.4093(4)	0.0573(1)	0.2110(3)	1.41(5)
TB′	0.4091(4)	0.4425(1)	0.2107(3)	1.40(5)
TC	0.5550(4)	0.1583(1)	0.5335(3)	1.37(5)
TC′	0.5539(3)	0.3421(1)	0.5333(3)	1.32(5)

TABLE 4.—*Continued*

Atom	x	y	z	B_{eq} (Å²)
		{010} sector		
TD	0.9065(3)	0.0527(1)	0.6415(3)	1.39(5)
TD′	0.9060(3)	0.4474(1)	0.6417(3)	1.37(5)
O1	0.3532(9)	0.1051(3)	0.0310(7)	1.9(1)
O1′	0.3533(9)	0.3945(3)	0.0315(7)	1.9(1)
O2	0.4240(9)	0.1249(4)	0.3562(8)	2.7(2)
O2′	0.4246(9)	0.3753(4)	0.3576(8)	2.6(2)
O3	0.7851(9)	0.1226(4)	0.5479(8)	2.3(1)
O3′	0.7820(9)	0.3780(4)	0.5465(8)	2.2(1)
O4	0.4457(9)	0.1400(4)	0.7130(8)	2.5(2)
O4′	0.4450(9)	0.3604(4)	0.7114(8)	2.5(2)
O5	0.0814(9)	0.0898(4)	0.7689(8)	2.5(2)
O5′	0.0798(9)	0.4098(4)	0.7677(8)	2.4(1)
O6	0.2313(10)	0.9977(4)	0.2417(9)	3.1(2)
O6′	0.2309(10)	0.5020(4)	0.2423(9)	3.0(2)
O7	0.3829(8)	0.9899(3)	0.7967(7)	1.9(1)
O7′	0.3827(9)	0.5105(3)	0.7964(8)	2.0(1)
O8	0	0	½	3.8(3)
O8′	0	½	½	3.5(3)
O9	0.568(1)	0.2503(4)	0.5011(9)	2.9(2)
M	0.2495(1)	0.24969(4)	0.17696(9)	1.26(1)
O10	0.056(1)	0.2497(5)	0.4676(9)	4.1(2)
O11	0.931(1)	0.1470(5)	0.147(1)	5.6(3)
O11′	0.930(1)	0.3527(5)	0.148(1)	5.6(3)
O12	0.603(1)	0.2493(5)	0.029(1)	5.2(2)
O13	0.076(1)	0.2495(4)	0.8628(9)	4.8(2)

Note: Refined M-site contents: {011} sector = $Sr_{0.50}Ba_{0.45}K_{0.01}$, {610} sector = $Sr_{0.40}Ba_{0.55}K_{0.01}$, and {010} sector = $Sr_{0.67}Ba_{0.24}K_{0.01}$. O10–O13 are H_2O O atoms.

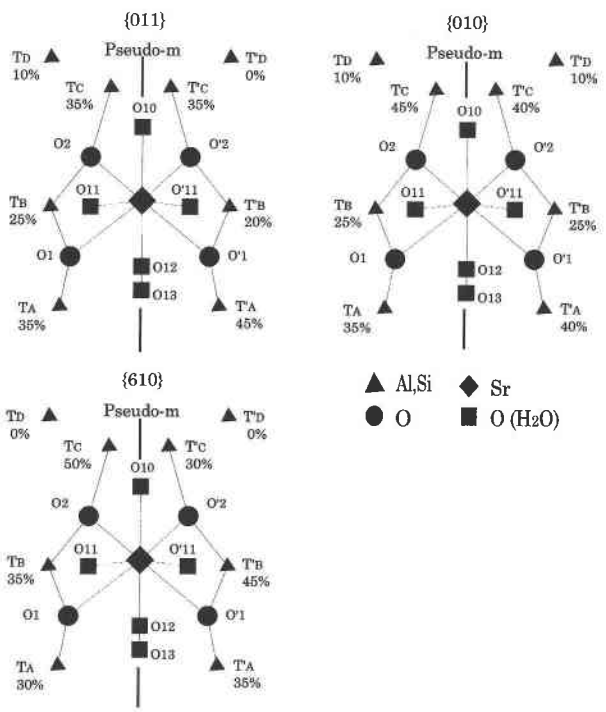

FIGURE 3. Schematic representations of Al occupancies, estimated from the method of Smith (1974), at the tetrahedral sites (T) around the Sr atom for the {011}, {610}, and {010} sectors. View is down the *a* axis. The pseudomirror plane (Pseudo-m) is vertical. Al occupancies estimated using the method of Artioli et al. (1985) are given in Table 7.

TABLE 6. Selected interatomic distances (Å) and bond angles (°)

{011} sector			
Tetrahedron		**Cation**	
TA-O1	1.658(5)	M-O1	2.894(5)
TA′-O1′	1.674(5)	M-O1′	2.876(5)
TA-O4	1.638(5)	M-O2	2.815(5)
TA′-O4′	1.646(5)	M-O2′	2.809(5)
TA-O5	1.653(5)	M-O10	2.685(6)
TA′-O5′	1.663(5)	M-O11	2.796(7)
TA-O7	1.655(5)	M-O11′	2.817(7)
TA′-O7′	1.662(5)	M-O12	2.707(6)
		M-O13	2.603(6)
TB-O1	1.650(5)		
TB′-O1′	1.641(5)	**Angles**	
TB-O2	1.623(5)	TB-O1-TA	133.6(3)
TB′-O2′	1.618(5)	TB′-O1′-TA′	133.9(3)
TB-O6	1.627(5)	TB-O2-TC	145.6(3)
TB′-O6′	1.628(5)	TB′-O2′-TC′	145.0(3)
TB-O7	1.637(5)	TD-O3-TC	139.3(3)
TB′-O7′	1.635(5)	TD′-O3′-TC′	139.3(3)
TC-O2	1.675(5)	TA-O4-TC	150.3(4)
TC′-O2′	1.685(5)	TA′-O4′-TC′	149.8(4)
TC-O3	1.659(5)	TD-O5-TA	138.8(4)
TC′-O3′	1.663(5)	TD′-O5′-TA′	139.5(3)
TC-O4	1.644(5)	TD-O6-TB	156.2(4)
TC′-O4′	1.635(5)	TD′-O6′-TB′	157.8(4)
TC-O9	1.627(6)	TB-O7-TA	136.1(3)
TC′-O9	1.625(6)	TB′-O7′-TA′	136.2(3)
		TD-O8-TD′	180
TD-O3	1.632(5)	TC-O9-TC′	162.2(4)
TD′-O3′	1.620(5)		
TD-O5	1.628(5)		
TD′-O5′	1.613(5)		
TD-O6	1.602(5)		
TD′-O6′	1.589(5)		
TD-O8	1.599(2)		
TD′-O8′	1.594(2)		

{610} sector			
Tetrahedron		**Cation**	
TA-O1	1.647(5)	M-O1	2.904(5)
TA′-O1′	1.653(5)	M-O1′	2.868(4)
TA-O4	1.629(5)	M-O2	2.826(5)
TA′-O4′	1.649(5)	M-O2′	2.832(5)
TA-O5	1.644(5)	M-O10	2.703(6)
TA′-O5′	1.651(5)	M-O11	2.832(7)
TA-O7	1.645(5)	M-O11′	2.858(7)
TA′-O7′	1.645(5)	M-O12	2.756(6)
		M-O13	2.651(6)
TB-O1	1.662(5)		
TB′-O1′	1.675(5)	**Angles**	
TB-O2	1.645(5)	TB-O1-TA	134.3(3)
TB′-O2′	1.659(5)	TB′-O1′-TA′	132.8(3)
TB-O6	1.646(5)	TB-O2-TC	145.4(3)
TB′-O6′	1.660(5)	TB′-O2′-TC′	145.6(3)
TB-O7	1.651(5)	TD-O3-TC	139.3(3)
TB′-O7′	1.661(5)	TD′-O3′-TC′	140.5(3)
TC-O2	1.676(5)	TA-O4-TC	146.6(3)
TC′-O2′	1.655(5)	TA′-O4′-TC′	147.2(3)
TC-O3	1.681(5)	TD-O5-TA	142.2(3)
TC′-O3′	1.665(5)	TD′-O5′-TA′	141.0(3)
TC-O4	1.662(5)	TD-O6-TB	153.0(4)
TC′-O4′	1.630(5)	TD′-O6′-TB′	151.7(4)
TC-O9	1.654(5)	TB-O7-TA	136.5(3)
TC′-O9	1.622(5)	TB′-O7′-TA′	136.7(3)
		TD-O8-TD′	180
TD-O3	1.610(5)	TC-O9-TC′	159.1(3)
TD′-O3′	1.610(5)		
TD-O5	1.606(5)		
TD′-O5′	1.609(5)		
TD-O6	1.592(5)		
TD′-O6′	1.589(5)		
TD-O8	1.594(2)		
TD′-O8′	1.596(2)		

TABLE 6.—*Continued*

{010} sector			
Tetrahedron		**Cation**	
TA-O1	1.670(6)	M-O1	2.886(6)
TA′-O1′	1.675(6)	M-O1′	2.886(6)
TA-O4	1.638(6)	M-O2	2.807(7)
TA′-O4′	1.641(6)	M-O2′	2.823(7)
TA-O5	1.646(6)	M-O10	2.688(7)
TA′-O5′	1.655(6)	M-O11	2.809(9)
TA-O7	1.652(6)	M-O11′	2.818(9)
TA′-O7′	1.660(6)	M-O12	2.732(8)
		M-O13	2.622(8)
TB-O1	1.647(6)		
TB′-O1′	1.643(6)	**Angles**	
TB-O2	1.633(6)	TB-O1-TA	133.3(4)
TB′-O2′	1.636(6)	TB′-O1′-TA′	133.1(4)
TB-O6	1.627(6)	TB-O2-TC	144.6(4)
TB′-O6′	1.630(6)	TB′-O2′-TC′	145.2(4)
TB-O7	1.640(6)	TD-O3-TC	138.9(4)
TB′-O7′	1.639(6)	TD′-O3′-TC′	139.2(4)
TC-O2	1.684(6)	TA-O4-TC	147.8(5)
TC′-O2′	1.668(6)	TA′-O4′-TC′	148.4(5)
TC-O3	1.679(6)	TD-O5-TA	140.4(4)
TC′-O3′	1.667(6)	TD′-O5′-TA′	140.2(4)
TC-O4	1.654(6)	TD-O6-TB	154.4(5)
TC′-O4′	1.643(6)	TD′-O6′-TB′	154.7(5)
TC-O9	1.638(7)	TB-O7-TA	136.1(4)
TC′-O9	1.632(7)	TB′-O7′-TA′	135.8(4)
		TD-O8-TD′	180.0
TD-O3	1.618(6)	TC-O9-TC′	160.8(4)
TD′-O3′	1.625(6)		
TD-O5	1.621(6)		
TD′-O5′	1.615(6)		
TD-O6	1.612(7)		
TD′-O6′	1.607(6)		
TD-O8	1.601(2)		
TD′-O8′	1.601(2)		

Note: Refined M-site contents: {011} sector = $Sr_{0.50}Ba_{0.45}K_{0.01}$, {610} sector = $Sr_{0.40}Ba_{0.55}K_{0.01}$, and {010} sector = $Sr_{0.67}Ba_{0.24}K_{0.01}$. O10–O13 are H_2O O atoms.

The (610) face consists of rough striations parallel to the c axis, on which vicinal faces are inclined toward the mirror plane. Al occupancy is larger in the TC site than in the TC′ site, and therefore the symmetry of the {610} sector is triclinic.

The vicinal faces on the (010) surfaces are slightly inclined toward the mirror plane. In the {010} sector, Al occupancies are larger in the TA′ and TC sites than in the TA and TC′ sites. Hence, the symmetry of the sector is triclinic as well.

Because the {010} sector occupies a large portion of the crystal volume, it is likely that both Perrotta and Smith (1964) and Schlenker et al. (1977) analyzed the {010} sector, the structure of which is nearly monoclinic. In addition, the diffraction maxima of $0k0$ ($>3\sigma$, k = odd) are weak and not easily observed.

Aluminosilicates that grow at low temperature show various sectoral textures. Their optical and X-ray symmetries are commonly lower than their morphological symmetry. Examples include triclinic chabazite (Akizuki 1981a; Smith et al. 1964), tetragonal and orthorhombic analcime (Akizuki 1981b; Mazzi and Galli 1978), and orthorhombic stilbite (Akizuki and Konno 1985; Akizuki et al. 1993). Edingtonite has been observed to consist of tetragonal and orthorhombic sectors (Akizuki 1986; Maz-

TABLE 7. Estimated Al contents (%) and averaged T-O distances (Å) in the T sites

	{011} sector	Al*	Al**	{610} sector	Al*	Al**	{010} sector	Al*	Al**	Schlenker et al. (1977)	
TA	1.651(5)	35	35	1.641(5)	30	25	1.652(6)	35	35	1.645(4)	<30%
TA′	1.661(5)	45	40	1.650(5)	35	30	1.658(6)	40	40		
TB	1.634(5)	25	20	1.651(5)	35	35	1.637(6)	25	20	1.664(4)	<40%
TB′	1.631(5)	20	20	1.664(5)	45	45	1.637(6)	25	20		
TC	1.651(5)	35	40	1.668(5)	50	50	1.664(6)	45	50	1.660(4)	<40%
TC′	1.652(5)	35	40	1.643(5)	30	30	1.653(6)	40	40		
TD	1.615(4)	10	10	1.601(4)	0	0	1.613(5)	10	5	1.607(4)	~0%
TD′	1.604(4)	0	0	1.601(4)	0	0	1.612(5)	10	5		

Note: The uncertainties in Al contents are ±5%, on the basis of the deviations of T-O bond length.
* Al contents estimated using the method of Smith (1974).
** Al contents estimated using the method of Artioli et al. (1985).

zi et al. 1984; Grice et al. 1984), although they are actually triclinic. Also, triclinic and monoclinic adularia crystals have been found to consist of fine-scale sectors corresponding to surface-growth features (Akizuki and Sunagawa 1978). The origins of the lower symmetries of these crystals were explained by a mechanism similar to that described for brewsterite. It is possible that most zeolites show anomalous optical properties indicating lower symmetry. The lower symmetries, however, are apparently produced by crystal growth, rather than by strain in the crystal.

ACKNOWLEDGMENTS

We thank two anonymous reviewers for their critical reviews and comments.

REFERENCES CITED

Akizuki, M. (1981a) Origin of optical variation in chabazite. Lithos, 14, 17–21.
——— (1981b) Origin of optical variation of analcime. American Mineralogist, 66, 403–409.
——— (1986) Al-Si ordering and twinning in edingtonite. American Mineralogist, 71, 1510–1514.
——— (1987a) Crystal symmetry and order-disorder structure of brewsterite. American Mineralogist, 72, 645–648.
——— (1987b) An explanation of optical variation in yugawaralite. Mineralogical Magazine, 51, 615–620.
Akizuki, M., and Sunagawa, I. (1978) Study of the sector structure in adularia by means of optical microscopy, infra-red absorption, and electron microscopy. Mineralogical Magazine, 43, 237–241.
Akizuki, M., and Konno, H. (1985) Order-disorder structure and the internal texture of stilbite. American Mineralogist, 70, 814–821.
Akizuki, M., Kudoh, Y., and Satoh, Y. (1993) Crystal structure of the orthorhombic {001} growth sector of stilbite. European Journal of Mineralogy, 5, 839–843.
Artioli, G., Smith, J.V., and Kvick, Å. (1985) Multiple hydrogen positions in the zeolite brewsterite $(Sr_{0.95}Ba_{0.05})Al_2Si_6O_{16}\cdot 5H_2O$. Acta Crystallographica, C42, 492–497.
Brooke, H.J. (1822) On the comptonite of Vesuvius, the brewsterite of Scotland, the stilbite and the heulandite. Edinburgh Philosophical Journal, 6, 112–115.
Cabella, R., Lucchetti, G., Palenzona, A., Quartieri, S., and Vezzalini, G. (1993) First occurrence of a Ba-dominant brewsterite: Structure features. European Journal of Minerals, 5, 353–360.
Des Cloizeaux, A. (1874) Manual de mineralogie, p. 420–422. Dunod, Editeur, Paris.
Grice, J.D., Gault, R.A., and Arsell, H.G. (1984) Edingtonite: The first two Canadian occurrences. Canadian Mineralogist, 22, 253–258.
Mazzi, F., and Galli, E. (1978) Is each analcime different? American Mineralogist, 63, 448–460.
Mazzi, F., Galli, E., and Gottardi, G. (1984) Crystal structure refinements of two tetragonal edingtonites. Neues Jahrbuch für Mineralogie Monatschefte, 373–382.
Perrotta, A.J. (1967) The crystal structure of epistilbite. Mineralogical Magazine, 36, 480–490.
Perrotta, A.J., and Smith, J.V. (1964) The crystal structure of brewsterite, $(Sr,Ba,Ca)(Al_2Si_6O_{16})\cdot 5H_2O$. Acta Crystallographica, 17, 857–862.
Robinson, G.W., and Grice, J.D. (1993) The barium analog of brewsterite from Harrisville, New York. Canadian Mineralogist, 31, 687–690.
Schlenker, J.L., Pluth, J.J., and Smith, J.V. (1977) Refinement of the crystal structure of brewsterite. Acta Crystallographica, B33, 2907–2910.
Smith, J.V. (1974) Feldspar minerals, 1, p. 627. Springer-Verlag, Heidelberg.
Smith, J.V., Knowles, C.R., and Rinaldi, F. (1964) Crystal structures with a chabazite framework, III. Acta Crystallographica, 17, 374–384.
teXsan (1985, 1992) Crystal structure analysis package. Molecular Structure Corporation, Texas.

MANUSCRIPT RECEIVED MAY 29, 1995
MANUSCRIPT ACCEPTED AUGUST 5, 1996